^{207}Pb NMR study of the relaxor behavior in $PbMg_{1/3}Nb_{2/3}O_3$

R. Blinc, A. Gregorovič, B. Zalar, and R. Pirc
Jožef Stefan Institute, P.O. Box 3000, 1001 Ljubljana, Slovenia

V. V. Laguta and M. D. Glinchuk
Institute for Material Sciences, Ukrainian Academy of Sciences, 03142 Kiev, Ukraine

(Received 23 June 2000; revised manuscript received 22 August 2000; published 14 December 2000)

The local structure of the relaxor single crystal PMN has been studied via a measurement of the temperature dependences of the ^{207}Pb spectra and relaxation times between 450 K and 15 K. The ^{207}Pb NMR spectra are frequency distributions which reflect the existence of polar nanoclusters and which can be well described by the recently proposed spherical random-bond–random-field model. The temperature dependence of the Edwards-Anderson order parameter q has been determined together with the random bond coupling and the random field variance. The results agree with those obtained from the ^{93}Nb NMR spectra and show that at any given instant of time the crystal consists of polar clusters with variable orientation and magnitude of the local polarization. The polar clusters are on the NMR time scale 10^{-4}–10^{-5} s, dynamic entities which exist for a certain amount of time, disappear, and then reappear in a different form.

DOI: 10.1103/PhysRevB.63.024104 PACS number(s): 77.84.Dy, 76.60.−k, 61.43.−j

I. INTRODUCTION

Lead magnesium niobate, $PbMg_{1/3}Nb_{2/3}O_3$ (PMN), is probably the best investigated perovskite relaxor crystal. According to x-ray studies[1] it has a cubic perovskite structure with the space group $Pm\bar{3}m$ in the whole investigated temperature range between 1000 K and 4 K. Structural refinement results have, however, shown that the local structure is different from the average structure. The ^{207}Pb atoms lie on their ideal cubic perovskite positions only above 925 K,[1] i.e., in a temperature range where the first-order Raman spectrum vanishes.[2] Burns and Dacol suggested that local and randomly oriented polar regions appear below this temperature demonstrating a disorder in the ^{207}Pb and ^{93}Nb positions[3] which increases with decreasing temperature. The size of these polar regions should be smaller than 500 Å so that they cannot be seen on the profile of the x-ray diffraction lines.[1,3] It has been suggested that the ^{207}Pb atoms shift by about 0.33 Å along the face diagonals [110], leading to 12 disordered ion sites around their special positions. The corresponding ^{93}Nb shifts should be about 0.18 Å along the face diagonals [110] or body diagonals [111], leading to 12 and eight, respectively, disordered sites around the special positions. Recent studies have, on the other hand, shown[4] that the ^{207}Pb ions are below 650 K, uniformly distributed over spherical shells around their special positions. The mean radial displacement is of the order of 0.33–0.4 Å.

Up to now the microscopic structural changes and ion displacements leading to the giant dielectric anomaly, characterizing the relaxor freezing around 0 °C, are still not completely understood. Until recently it has not been definitely known whether the relaxor state in PMN in zero field is a ferroelectric phase broken up into nanodomains under the constraint of quenched random fields[5,6] or whether it is a kind of a dipolar glass state with randomly interacting polar microregions.[7] Recent high-resolution measurements of the temperature dependence of the dielectric nonlinearities seem, however, to show[8] a behavior typical of glasses rather than ferroelectrics in random field.

A number of important questions, however, still remain open. The first is, what kind of glass are relaxors? Are they similar to dipolar glasses where elementary dipoles exist on an atomic scale or is the relaxor state indeed characterized by the presence of nanosized polar clusters of variable sizes and orientations? If this last case is correct, relaxors cannot be described by a discrete ordering field of fixed length as in, say, Ising-type dipolar glasses. Rather they represent a new kind of glass with a quasicontinuous order parameter field,[9] which is related to the polarization of the polar clusters. Another important open problem is the nature of nonpolar matrix into which polar clusters are assumed to be embedded. Are the polar clusters and the nonpolar matrix dynamic or static entities?

To throw some additional light on the above questions we decided to perform a ^{207}Pb NMR study of the relaxor transition in a PMN single crystal at a magnetic field of 9.1 T. We particularly wished to check the local structure of PMN and the recently proposed spherical random-bond–random-field (SRBRF) model of relaxor $AB_x^{\mathrm{I}}B_{1-x}^{\mathrm{II}}O_3$ ferroelectrics[9] with a magnetic resonance study of an A-site nucleus which does not exhibit substitutional disorder. The SRBRF model has been so far tested only by B-site ion NMR where we have $B^{\mathrm{I}} \leftrightarrow B^{\mathrm{II}}$ cationic substitutional disorder.

The use of high magnetic fields is essential for the study of the ^{207}Pb NMR spectra. The ^{207}Pb($I=1/2$) nucleus has no electric quadrupole moment, unlike the ^{93}Nb nucleus, but exhibits a large chemical shift tensor anisotropy. The ^{207}Pb nucleus is thus in contrast to the ^{93}Nb($I=9/2$) nucleus—which has a large quadrupole moment and ''feels'' the electric field gradient of the surrounding ions—a purely local probe. It is thus mainly sensitive to the local ^{207}Pb displacements from their cubic special positions. The size of the NMR frequency shifts reflecting the ^{207}Pb ion displacements and thus the sensitivity of the NMR technique is here the higher the larger the value of the applied external magnetic field.

The ^{207}Pb results are compared with ^{93}Nb($I=9/2$) $1/2\leftrightarrow -1/2$ quadrupole perturbed NMR spectra which reflect the changes in the central part of the oxygen octahedron, i.e., at the *B* sites.

II. EXPERIMENT

A. NMR

The ^{207}Pb($I=1/2$) spin-echo Fourier transform NMR spectra of an optically pure PMN single crystal have been measured in a wide bore superconducting magnet at a Larmor frequency ν_L(Pb)=79.4 MHz. The width of the 90° pulse was 4 μs. The orientation of the crystal was determined by x rays. The quadrupole perturbed ^{93}Nb $1/2\leftrightarrow -1/2$ NMR spectra were measured at ν_L(Nb)=92.9 MHz. The satellite $3/2\leftrightarrow 1/2$, $5/2\leftrightarrow 3/2$, $7/2\leftrightarrow 5/2$, and $9/2\leftrightarrow 7/2$ spectra are not well resolved and contribute to the several MHz broad background component on which the relatively narrow $1/2\leftrightarrow -1/2$ component is superimposed.

The temperature dependences of the ^{207}Pb and ^{93}Nb spin-lattice relaxation rates were measured with the saturation–spin-echo sequence $90^\circ_x \cdots 90^\circ_x \cdots 90^\circ_x \cdots -\tau - 90^\circ_y - 180^\circ$.

^{207}Pb chemical shifts are expressed with respect to the Pb-nitrate water solution. A $3\times3\times2$ mm^3 crystal with well-developed faces has been used.

B. Chemical ordering

Relaxors are materials with more than one kind of ion at otherwise equivalent positions. The degree of substitutional order and/or disorder clearly affects the NMR spectra as it produces chemically different environments for different nuclear sites.

Annealing of the material at high enough temperatures induces chemical ordering[11–13] and usually leads to the formation of a hybrid phase where chemically ordered and disordered domains coexist. These domains are *T* independent and static below 950 °C. As-grown PMN crystals are usually homogeneously chemically disordered. They may, however, also show a hybrid behavior with a small amount of an ordered phase.

There are several different models of chemical ordering in PMN. According to the so called ''space charge'' model[12]—which is by now discarded[13]—one has a 1:1 cation ordering where Nb-''poor'' domains with a composition $[Pb(Mg_{1/2}Nb_{1/2})O_3]^{0.5-}$ are surrounded by an oppositely charged, Nb-''rich'' disordered matrix.

In the layer type variant of this space charge model of chemical ordering the ordered Nb-rich $Pb^{2+}Nb^{5+}O_3{}^{2-}$ and Nb-poor $Pb^{2+}Mg_{1/2}{}^{2+}Nb_{1/2}{}^{5+}O_3{}^{2-}$ regions alternate. In the disordered version of this model the sequence of Nb-rich and the Nb-poor regions is random as well as the distribution of the Mg^{2+} and Nb^{5+} ions among the ''cationic'' sites in the Nb-poor layers.

According to the ''charge-balanced'' random layer model we have alternating Nb-rich $Pb^{2+}Nb^{5+}O_3{}^{2-}$ and Nb-poor $Pb^{2+}Mg_{2/3}{}^{2+}Nb_{1/3}{}^{5+}O_3{}^{2-}$ layers. The disordered version of this model again assumes the existence of a random distribution of Nb-rich and Nb-poor layers and/or a random 2:1 distribution of the cations between the B^{I} and B^{II} sites in the Nb-poor layers.

The common point of all these models is that we have more than one chemically different Pb^{2+} and Nb^{5+} site even in the case of chemical ordering. Ion-site disorder will produce additional differences among the cations.

III. SPHERICAL VECTOR GLASS MODEL AND NMR SPECTRA

A. SRBRF model

Superimposed on the substitutional disorder of the B^{I} and B^{II} ions is the disorder due to the distribution of a given kind of ions between different off-center sites surrounding a given high-symmetry perovskite lattice position. The correlated motion of these ions gives rise to reorientable polar clusters even far above the relaxor transition temperature. The polar clusters are expected to be dynamic entities embedded in a polarizable matrix. They vary both in size and in orientation of the local polarization. Recently the SRBRF model has been introduced[9] where the order parameter field is described as a continuous vector of variable length which is associated with the dipole moment of interacting reorientable polar clusters. This is quite different from the assumption of a fixed length order parameter field typically made for Ising-type dipolar glasses or quadrupole glasses. Within the SRBRF model relaxors thus correspond to a new type of glass, namely, the spherical vector glass. For such a glass,[9] the nonlinear dielectric anomaly $a_3=\chi_3/\epsilon_S^4$ should increase on approaching the relaxor freezing temperature T_f from above, whereas it should decrease on approaching T_f if we deal with a ferroelectric broken up into nanodomains under the constraint of quenched random fields.[9] Here χ_3 is the third-order nonlinear susceptibility and ϵ_S the static-field-cooled dielectric constant.

The SRBRF model Hamiltonian of a system of interacting polar clusters can be written as

$$\mathcal{H}=-\sum_{i<j} J_{ij}\vec{S}_i\cdot\vec{S}_j-\sum_i \vec{h}_i\cdot\vec{S}_i, \tag{1}$$

where the J_{ij} and $\vec{h}_i$ are random interactions constants and random fields, respectively.[9] Here $\vec{S}_i$ is proportional to the polar cluster dipole moment and scales with the cluster size. It is in fact a discrete vector of variable length restricted to a large but finite number of equilibrium orientations. In the simplest case we can assume that each component fluctuates continuously,

$$-\infty<S_{i\mu}<+\infty, \quad \mu=x,y,z, \tag{2}$$

subject to the closure relation

$$\sum_i \vec{S}_i^2=3N, \tag{3}$$

where N is the total number of reorientable polar clusters. The J_{ij} couplings are assumed to be infinitely ranged with a Gaussian distribution characterized by cumulant averages $[J_{ij}]^c_{\rm av}=J_0/N$ and $[J_{ij}^2]^c_{\rm av}=J^2/N$. The random field distribu-

tion is similarly assumed to be Gaussian but with a zero mean value. The variance of the random field distribution is $[h_{i\mu}h_{j\nu}]^c_{\rm av}=\delta_{ij}\delta_{\mu\nu}\Delta$.

In the fast motion limit the NMR nucleus does not ''see'' the instantaneous value of the ordering field $\vec{S}_i$ but its time average $\vec{p}_i=\langle\vec{S}_i(t)\rangle$ which can be replaced by the thermodynamic average

$$\vec{p}_i=\langle\vec{S}_i\rangle. \tag{4}$$

Here $\vec{p}_i$ is the local polarization.

The local polarization distribution function can be now expressed[9,10] as

$$W(\vec{p})=\frac{1}{N}\sum_i\ \delta(\vec{p}-\vec{p}_i)=w(p_x)w(p_y)w(p_z). \tag{5}$$

For $J>J_0$ there is no long-range order and one finds

$$w(p_\mu)=\frac{1}{\sqrt{2\pi q}}\exp\left(-\frac{p_\mu^2}{2q}\right), \tag{6a}$$

whereas

$$W(\vec{p})=\frac{1}{\sqrt{(2\pi q)^3}}\exp\left(-\frac{\vec{p}^2}{2q}\right). \tag{6b}$$

Here q is the spherical glass Edwards-Anderson order parameter. According to the SRBRF model $W(\vec{p})$ is thus Gaussian at all temperatures and its width is determined by q.

B. NMR line shapes

The NMR frequency of a quadrupole or chemical shift perturbed nucleus at site i depends in the fast motion limit on the local polarization

$$\nu_i=\nu(\vec{p}_i). \tag{7}$$

This relation can be expanded in a power series

$$\nu_i(\vec{p}_i)=\nu_0+\vec{\alpha}\cdot\vec{p}_i+\vec{p}_i\cdot\boldsymbol{\beta}\cdot\vec{p}_i+\cdots, \tag{8}$$

where the coefficients $\vec{\alpha}$ and $\boldsymbol{\beta}$ depend on the orientation of the external magnetic field with respect to the principal axes of the electric field gradient (EFG) or chemical shift tensors (see Sec. III C). The inhomogeneous NMR line shape

$$f(\nu)=\frac{1}{N}\sum_i\ \delta(\nu-\nu_i) \tag{9}$$

can be now related to $W(\vec{p})$ as

$$f(\nu)=\int d^3p\,W(\vec{p})\,\delta(\nu-\nu_0-\vec{\alpha}\cdot\vec{p}-\vec{p}\cdot\boldsymbol{\beta}\cdot\vec{p}). \tag{10}$$

In the linear case, $|\vec{\alpha}|\gg\|\boldsymbol{\beta}\|$, the line shape is Gaussian,

$$f(\nu)=\frac{1}{\sqrt{2\pi q\alpha^2}}\exp\left[-\frac{(\nu-\nu_0)^2}{2q\alpha^2}\right], \tag{11}$$

and the second moment of $f(\nu)$ is just $M_2=q\alpha^2$.

In the bilinear case $|\vec{\alpha}|\ll\|\boldsymbol{\beta}\|$, the line shape is asymmetric. For

$$\boldsymbol{\beta}=\beta_0\begin{pmatrix}1&0&0\\0&0&0\\0&0&0\end{pmatrix} \tag{12a}$$

in particular we find a singularity in $f(\nu)$ at $\nu=\nu_0$, i.e., at $p=0$:

$$f(\nu)=\Theta(\nu-\nu_0)\frac{1}{\sqrt{2\pi q\beta_0(\nu-\nu_0)}}\exp\left[-\frac{1}{2}\frac{(\nu-\nu_0)}{q\beta_0}\right],$$

$$\beta_0>0. \tag{12b}$$

Here $\Theta(x)$ is the unit step function. For $\beta_0<0$, $f(\nu)$ is mirrored around $\nu=\nu_0$.

The glass order parameter is here related to the first moment of $f(\nu)$ as $M_1=\beta_0 q$. In the slow motion limit (see the Appendix), on the other hand, the inhomogeneous NMR line shape reflects the instantaneous distribution of the $\vec{S}_j$ amplitudes and orientations:

$$\nu_i=\nu_i(\vec{S}_j). \tag{13}$$

C. ^{207}Pb chemical shift anisotropy and the NMR line shapes in a crystal with average cubic symmetry

Let us now apply the SRBRF model to evaluate the ^{207}Pb NMR line shape in PMN in more detail. We assume that the ^{207}Pb nuclei are displaced from their high-symmetry perovskite sites so that the average cubic symmetry is locally broken. The ^{207}Pb chemical shift tensors $\boldsymbol{\sigma}$ are thus anisotropic and can be written as a sum of a scalar part σ_0 and a traceless second-rank tensor part $\boldsymbol{\sigma}_a$:

$$\boldsymbol{\sigma}=\sigma_0\mathbf{1}+\boldsymbol{\sigma}_a. \tag{14}$$

We further assume that $\boldsymbol{\sigma}_a$ possesses cylindrical symmetry as appropriate for tetragonal or trigonal local distortions and can be expressed in its eigenframe as

$$\boldsymbol{\sigma}_a=\begin{pmatrix}-\sigma_a/2&0&0\\0&-\sigma_a/2&0\\0&0&\sigma_a\end{pmatrix}. \tag{15}$$

In the fast-motion limit of the SRBRF model the largest principal axis of $\boldsymbol{\sigma}_a$ should be parallel to the direction of the polarization $\vec{p}_i$ of a given polar cluster i. As discussed in Sec. III E the chemical shift tensors $\boldsymbol{\sigma}$ occurring in expressions (14) and (15) are in the fast-motion limit weighted averages of tensors for a particular set of $\vec{S}_i$ values.

The largest principal value $\sigma_{a,i}$ in such a cluster will generally depend on the magnitude of the cluster polarization p and the direction of the effective, motionally averaged nuclear displacement, i.e., the orientation of the corresponding principal axis with respect to the crystal fixed frame determined by the angles ϑ and φ: $\sigma_a=\sigma_a(p,\vartheta,\varphi)$.

The nuclear spin Hamiltonian is in the present case a sum of nuclear Zeeman term $\mathcal{H}_Z$ and a chemical shift coupling term $\mathcal{H}_C$:

$$\mathcal{H}=\mathcal{H}_Z+\mathcal{H}_C, \tag{16a}$$

where

$$\mathcal{H}_Z=-\gamma_{Pb}\hbar\vec{I}\cdot\vec{B}_0 \tag{16b}$$

and

$$\mathcal{H}_C=-\gamma_{Pb}\hbar\vec{I}\cdot\boldsymbol{\sigma}\cdot\vec{B}_0. \tag{16c}$$

For a general orientation of the crystal with respect to the direction of the magnetic field $\vec{B}_0$ specified by $\{\theta,\phi\}$, the ^{207}Pb NMR transition frequencies will be given by

$$\nu_{Pb}=\nu_L[1+\sigma_0+\sigma_{zz}(p,\vartheta,\varphi,\theta,\phi)]. \tag{17}$$

ν_L is here the unperturbed Pb nuclear Larmor frequency, σ_0 the isotropic part of the chemical shift tensor, and σ_{zz} is the component of $\boldsymbol{\sigma}_a$ along the magnetic field direction. σ_{zz} is obtained by a double transformation, from the eigenframe to the crystal frame, and then from the crystal frame to the magnetic field fixed laboratory frame:

$$\sigma_{zz}(p,\vartheta,\varphi,\theta,\phi)=\sigma_a(p,\vartheta,\varphi)\frac{4\pi}{5}\times\sum_{m=-2}^{2}P_{2m}(\theta,\phi)P_{2m}(\vartheta,\varphi). \tag{18}$$

P_{2m} are here Legendre polynomials of order $l=2$.

$\sigma_a(p,\vartheta,\varphi)$ can be expanded in powers of the local polarization as

$$\sigma_a(p,\vartheta,\varphi)=\sigma_{a0}(\vartheta,\varphi)+\sigma_{a1}(\vartheta,\varphi)p+\sigma_{a2}(\vartheta,\varphi)p^2+\cdots. \tag{19a}$$

It is this term which describes the dependence of the coefficients $\vec{\alpha}$ and $\boldsymbol{\beta}$ in expression (8) on the crystal orientation $\{\vartheta,\varphi\}$ and is thus responsible for the domination of the linear term in p over the quadratic term (or vice versa) at a given orientation as described in Sec. III B. Here σ_{a0}, σ_{a1}, and σ_{a2} can be expanded in terms of cubic harmonics:

$$\sigma_{am}(\vartheta,\varphi)=C_0^{(m)}+C_4^{(m)}K_4(\cos\vartheta,\varphi)+C_6^{(m)}K_6(\cos\vartheta,\varphi)+\cdots, \tag{19b}$$

where $m=0,1,2$. Here $K_i(\cos\vartheta,\varphi)$ is a cubic harmonic of order i. It should be also noted that second-order terms $i=2$ are absent from this expansion.

The scalar part of the chemical shift tensor σ_0 can be, in principle, as well a function of the local polarization

$$\sigma_0=\sigma_{00}+\sigma_{01}p+\sigma_{02}p^2+\cdots. \tag{20}$$

It will, however, not contribute to the angular dependence of the NMR spectra as it will give the same values of the coefficient $\vec{\alpha}$ and $\boldsymbol{\beta}$ at any orientation of the crystal with respect to the magnetic field direction. The polarization dependence is here due to displacements from the positions of noncubic symmetry arising from substitutional disorder. The NMR line shape can be now determined if we know the distributions of the magnitudes and orientations of the local cluster polarizations $W(p,\vartheta,\varphi)$.

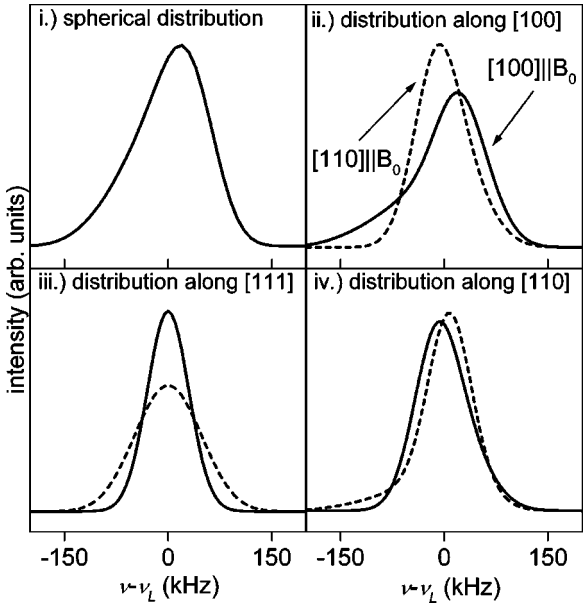

FIG. 1. Theoretical ^{207}Pb NMR line shapes for the case where $\sigma_a=\sigma_{a0}+\sigma_{a1}p$, the magnitude p follows a normal distribution, and the distribution of the longest principal axes of the σ_a tensor can be described with (i) a spherical distribution, (ii) a distribution along the [100] directions, or (iii) a distribution along the [111] directions and a distribution along the [110] directions. The orientation of the magnetic field is along the [100] direction (solid line) and [110] direction (dashed line).

Within the SRBRF model the angular distribution of the polarization vector possesses a spherical symmetry [see expression (6b)]. The distribution $\tilde{W}(p)$ of the magnitudes of the local polarizations therefore has a Maxwell type profile

$$\tilde{W}(p)=\frac{4\pi}{\sqrt{(2\pi q)^3}}p^2\exp\left(-\frac{p^2}{2q}\right). \tag{21}$$

The model of course allows that the instantaneous value of the local polarization points into certain preferred directions (e.g., along cubic axes). Because of fast exchange between many different possible ionic sites, however, the time-averaged value (or the thermodynamic expectation value) of the polarization can point into any direction with equal probability.

The NMR line shape $f(\nu,\theta,\phi)$ is now obtained for a given orientation $\{\theta,\phi\}$ of crystal in the external magnetic field as

$$f(\nu,\theta,\phi)=\int\int\int W(\vec{p})\,\delta\{1-\nu_L[1+\sigma_0(p)+\sigma_{zz}(p,\vartheta,\varphi,\theta,\phi)]\}p^2dp\,d(\cos)\vartheta\,d\varphi. \tag{22}$$

Its is obvious that as soon as local cubic symmetry breaking takes place, so that σ_a and thus also σ_{zz} are different from zero, the ^{207}Pb NMR line shape will be orientation dependent. In Fig. 1 the theoretical ^{207}Pb line shapes are presented for $\sigma_a=\sigma_{a0}+\sigma_{a1}p$ and for the following.

(i) A spherical distribution of the orientations of the longest principal axes of the σ_a tensor with the magnitudes of the axes following a normal distribution (SRBRF).

(ii) The case that the longest principal axes of the σ_a tensor point along [100], [010], [001], [$\bar{1}$00], [0$\bar{1}$0], and [00$\bar{1}$] directions, whereas the magnitudes of the axes follow a normal distribution. The magnetic field is oriented along [100] (solid line) and [110] (dashed line).

(iii) The case that the longest principal axes of the σ_a tensor point along [111], [11$\bar{1}$], [1$\bar{1}$1], [1$\bar{1}\bar{1}$], [$\bar{1}$11], [$\bar{1}\bar{1}$1], [$\bar{1}$1$\bar{1}$], and [$\bar{1}\bar{1}\bar{1}$] directions and the magnitudes of the axes follow a normal distribution. The magnetic field is oriented along [100] (solid line) and [110] (dashed line).

(iv) The case that the longest principal axes of the σ_a term point along [110], [1$\bar{1}$0], [$\bar{1}$10], [$\bar{1}\bar{1}$0], [101], [10$\bar{1}$], [$\bar{1}$01], [$\bar{1}$0$\bar{1}$], [011], [01$\bar{1}$], [0$\bar{1}$1], and [0$\bar{1}\bar{1}$] directions and the magnitudes of the axes follow a normal distribution. The magnetic field is oriented along [100] (solid line) and [110] (dashed line).

It should be noted that in case (i) the positions of the line as well as the line shape are not dependent on the direction of the magnetic field, whereas in cases (ii), (iii), and (iv) the line positions and line shape generally depend on the direction of the magnetic field with respect to the crystal axes.

It is interesting to compare the above results with the NMR line shape obtained for a simple isotropic distribution of the orientations of the longest principal axes of uniaxial ^{207}Pb chemical shift tensors which assumes that all these axes have the same magnitude. In such a case the distribution of magnitudes becomes

$$\tilde{W}(p)=\frac{1}{4\pi}\delta(p-p_0), \tag{23a}$$

and the average frequency is orientation independent:

$$\langle\nu\rangle=\nu_L(1+\sigma_0). \tag{23b}$$

The NMR line shape is here far from Gaussian. It is of the well-known[15] powderlike shape. The frequency distribution extends from the singularity at $\nu=\nu_L\sigma_a/2$ to the shoulder at $\nu=-\nu_L\sigma_a$ and is of course orientation independent.

D. Spin-lattice relaxation

For an ion jumping in an asymmetric double well in a polar cluster the spin-lattice relaxation rate will depend on the magnitude of the local polarization as

$$T_1^{-1}(p)\propto\frac{\tilde{\tau}}{1+(\omega\tilde{\tau})^2}(1-p^2), \tag{24}$$

with $\tilde{\tau}=\tau\sqrt{1-p^2}$ and $p=\tanh(\Delta U/2kT)$, where ΔU is the asymmetry of the double potential well. The spin-lattice relaxation rate will depend on the local polarization p also in the more general case of an ion moving in a multisite potential. Since the local polarization distribution function $W(\vec{p})$ is a Gaussian and not a δ function, we expect a variation of T_1 over the spectrum $f(\nu)$.

At any given frequency we have here a distribution of spin-lattice relaxation rates

$$F\left(\frac{1}{T_1},\nu\right)=\int d^3pW(\vec{p})\delta[\nu-\nu(\vec{p})]\delta\left[\frac{1}{T_1}-\frac{1}{T_1}(\vec{p})\right]. \tag{25}$$

The magnetization recovery will thus be in general nonexponential,

$$M(t)-M_0=M_0\int_0^\infty\hat{W}(T_1^{-1})\exp(-t/T_1)dT_1^{-1}, \tag{26}$$

and will be given by the Laplace transform of the relaxation time distribution function $\hat{W}(T_1^{-1})$. Here $\hat{W}(T_1^{-1})$ is $F(1/T_1,\nu)$ integrated over the frequency interval of interest.

The presence of a distribution of spin-lattice relaxation times in relaxors will thus show up in three different effects.

(1) The variation of T_1 over the inhomogeneous NMR frequency distribution $f(\nu)$.

(2) The nonexponential magnetization recovery.

(3) The asymmetric shape of the T_1 vs $1000/T$ temperature dependence: The slope of the T_1 vs $1000/T$ curve will be different on the high-T side of the T_1 minimum from that on the low-T side.

The above three effects should occur in addition to the intrinsic nonexponential magnetization recovery of quadrupolar nuclei after the saturation of the $1/2\leftrightarrow-1/2$ transition.

E. Effect of local polarization fluctuations on the NMR line shape

In the fast-motion limit the NMR nucleus in a given polarized cluster does not see the instantaneous value of the ordering field $\vec{S}_i$ but its time average $p_i=\langle\vec{S}_i(t)\rangle$. For the case of the ^{207}Pb($I=1/2$) NMR this means that a given nucleus sees the time average value of the chemical shift tensors corresponding to the sites the ion visits in a time shorter than the NMR time scale:

$$\bar{\boldsymbol{\sigma}}_a=\sum_k C_k\boldsymbol{\sigma}_{a,k}, \tag{27}$$

where $C_k=\tau_k/\Sigma_k\tau_k$ represents the fraction of time the nucleus spends at site k. The NMR time scale is here given by the inverse frequency separation between the ^{207}Pb Larmor frequencies at two different ionic sites. The expressions in Sec. III C thus all contain the time-averaged values of the chemical shift tensors. The braces have been omitted there for sake of simplicity.

When the lifetime of a given cluster becomes longer than the inverse frequency separation between NMR lines belonging to different clusters we come to the slow-motion limit

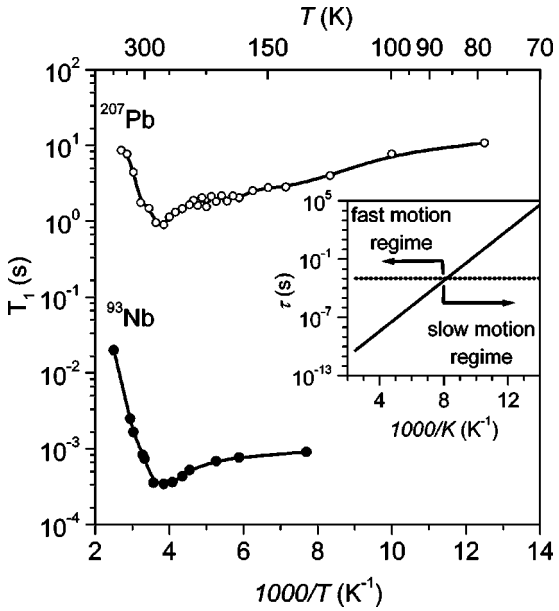

FIG. 2. T dependence of the ^{207}Pb and ^{93}Nb spin-lattice relaxation times T_1 in PMN. The inset shows the mean correlation time for the order parameter fluctuations τ extracted from the ^{207}Pb T_1 data (solid line) and the ^{207}Pb inverse rigid lattice linewidth (dotted line).

where the nucleus sees the instantaneous value of the ordering field. The NMR line shape for this case is treated in the Appendix.

The situation is somewhat more complicated in the case of quadrupolar nuclei such as ^{93}Nb($I=9/2$). Here we usually observe the central quadrupole perturbed $1/2\leftrightarrow -1/2$ transition which is shifted in second order only. In the representation of eigenstates the time-dependent perturbation $\mathcal{H}_1$ contains both diagonal and off-diagonal elements. It can be shown[16] that in such a case the time-dependent perturbation averages out in two steps at two different time scales, the Larmor frequency time scale and the much slower line splitting time scale. In the limit of very short correlation times, when the correlation time is much shorter than the inverse Larmor frequency, the $1/2\leftrightarrow -1/2$ transition is observed at a position which corresponds to the time-averaged Hamiltonian. The symmetry-breaking time-dependent perturbation $\mathcal{H}_1$ is here averaged out. In the limit of intermediate correlation times, when the correlation time is between the inverse Larmor frequency and the inverse line splitting, the time-dependent perturbation is only partially averaged out. The angular dependence of the shifts will be the one given by the perturbation $\mathcal{H}_1$ whereas the line splitting is still averaged out. When however the correlation time becomes longer than the inverse line splitting the resonance spectrum becomes the same as if the time-dependent perturbation were static.

IV. RESULTS AND DISCUSSION

A. Spin-lattice relaxation

The ^{207}Pb magnetization recovery curves are monoexponential $M(t)=M_0[1-\exp(-t/T_1)]$ at 420 K but become definitely nonexponential $M(t)=M_0[1-\exp(-t/T_1)^{\alpha}]$ below the relaxor transition, e.g., at 80 K.

The T dependences of the ^{207}Pb($I=1/2$) and ^{93}Nb ($I=9/2$) spin-lattice relaxation times are shown in Fig. 2. In both cases an asymmetric T_1 minimum is found in the region of the relaxor transition between 260 and 270 K. The minimum occurs in the region of the maximum of the imaginary part of the dielectric susceptibility χ''.[14] The T_1 minimum is thus related to electric dipolar reorientations which are presumably due to polar cluster fluctuations. At the T_1 minimum $T_1(^{207}\mathrm{Pb})_{\min}\approx 0.8$ s, whereas $T_1(^{93}\mathrm{Nb})_{\min}\approx 0.35$ ms is much shorter. The two minima are obviously due to the same relaxation mechanism, i.e., order parameter fluctuations. The fact that the ^{93}Nb T_1 minimum is much deeper than the ^{207}Pb one shows that ^{93}Nb quadrupolar fluctuations are much larger than ^{207}Pb chemical shift tensor fluctuations. This is indeed expected.

The occurrence of the T_1 minimum demonstrates that in this temperature range $\omega_L\tau\approx 1$, thus allowing for a determination of the temperature dependence of the mean correlation time τ for order parameter fluctuations (see the inset of Fig. 2). From the high-temperature part of the slope of the T_1 vs $1000/T$ dependence we obtain the activation energy for ionic jumps as ≈ 250 meV. The asymmetry of the T_1 minimum shows that we deal with a broad distribution of correlation times as indeed expected for relaxors. It should be noted that on the high-temperature side of the T_1 minimum where $\omega_L\tau\ll 1$, the distribution of τ values does not affect the T dependence of T_1 significantly. On the low-T side, on the other hand, the presence of a distribution of τ values is responsible for the slow increase in T_1 and the lower apparent activation energy. The description of the dynamical process with a single mean correlation time τ is thus only a very rough approximation. Nevertheless, it demonstrates the occurrence of a glasslike freezing at relaxor transition. It also allows one to conclude from the magnitude of τ and the width $\Delta\nu$ of the ^{207}Pb and ^{93}Nb $1/2\leftrightarrow -1/2$ NMR spectra that we are in the fast motion limit where $2\pi\Delta\nu\tau\ll 1$ at least above 80 K. In this range the nucleus ''sees'' the time average value of the order parameter field and we can use the local polarization distribution function $W(\vec{p})$ and the Edwards-Anderson order parameter q to describe the NMR spectra.

B. ^{207}Pb NMR spectra

The temperature dependence of the ^{207}Pb NMR line shape in PMN for the orientation $[001]\|\vec{B}_0$ is shown in Fig. 3. At high temperatures above 410 K the line shape is approximately Gaussian and independent of the orientation of the crystal in the magnetic field. Its shape and width are practically temperature independent at temperatures above 410 K. Its half-width is approximately 30 kHz. The width is much too large to be accounted for by nuclear magnetic dipolar interactions. We believe that the observed width is due to a distribution of isotropic chemical shifts due to the substitutional disorder. The corresponding local polarization is here very small and corresponds to a value of the Edwards-Anderson order parameter of about $q\approx 10^{-2}$. The local

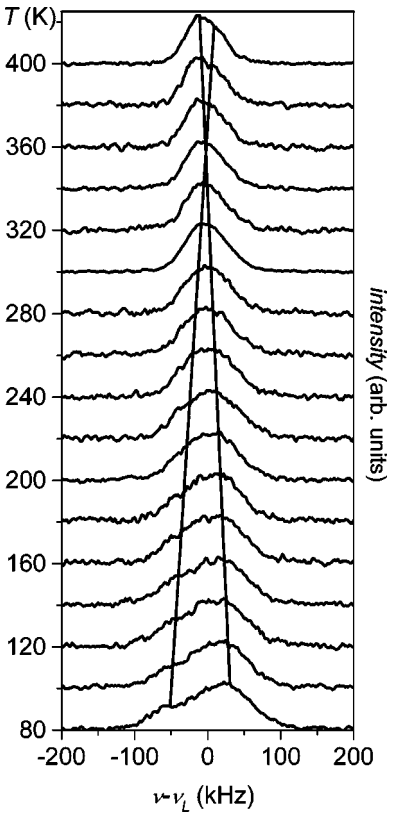

FIG. 3. Temperature dependence of ^{207}Pb NMR lineshape in PMN for the orientation $[001]\|\vec{B}_0$.

structure is thus here approximately cubic. A given nucleus spends most of its time in a nonpolar matrix and only a small fraction of time in a polar cluster [see expression (27)]. The comparison between the calculated and experimental line shapes at 410 K is shown in Fig. 4. The theoretical curve has been calculated according to Eq. (22) with $\sigma_{zz}=0$ and a Gaussian distribution of σ_0 so that Eq. (22) becomes

$$f(\nu,\theta,\phi)=\int \delta[1-\nu_L(1+\sigma_0)]\rho(\sigma_0)d\sigma_0, \qquad (28)$$

where $\rho(\sigma_0)$ is a Gaussian distribution with a mean $\overline{\sigma_0}=10^{-3}$ and a second moment 0.16×10^{-6}.

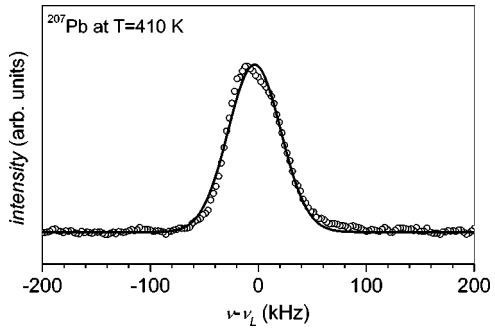

FIG. 4. Comparison between the theoretical (solid line) and experimental (open circles) ^{207}Pb line shape in PMN at 410 K at orientation $[001]||B_0$.

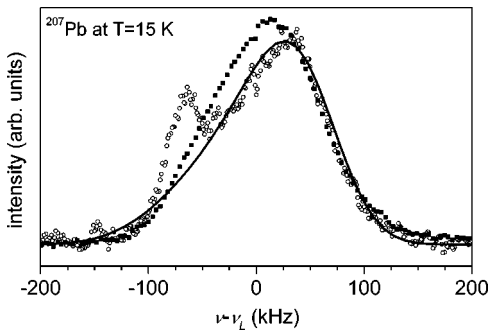

FIG. 5. NMR ^{207}Pb line shape at the orientations $[001]||B_0$ (open circles) and $[011]||B_0$ (solid squares) at the temperature 15 K.

On lowering the temperature the spectrum becomes broader and starts to depend on the orientation of the crystal in the magnetic field (Fig. 5). The spectrum also becomes slightly asymmetric. It can be decomposed into two slightly displaced Gaussian components [Fig. 6(a)] with an intensity ratio 4:1. The weaker component is orientation dependent and could be due to the chemically ordered part of the crystal. Here the ^{207}Pb displacements are not spherically distributed but are restricted to certain directions [see Fig. 1(ii)], giving rise to an angular dependence of the NMR line. The conclusion that the weaker line can be associated with the chemically ordered part of the crystal is also supported by the fact that in another sample which is presumably homogeneously disordered, this second (weaker) component is absent. The stronger component practically does not depend on the orientation of the crystal in the magnetic field, though it significantly broadens with decreasing temperature. On cooling from 410 K the centers of gravity of the two components first cross around 350 K and then slowly move apart. The temperature dependence of the centers of gravity of the two components is shown in Fig. 6(b) and the temperature dependence of the corresponding widths in Fig. 6(c).

The observed line shape at 410 K (Fig. 4) and 15 K (Fig. 5) has been compared with the predictions of two theoretical models. According to the first [Fig. 1(i)], all possible polar-

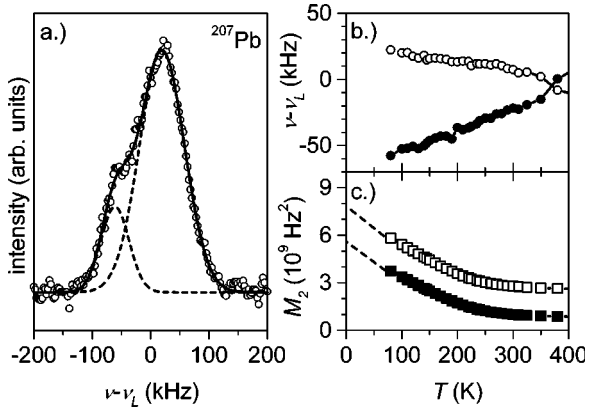

FIG. 6. (a) Decomposition of the ^{207}Pb NMR line shape in two components, (b) temperature dependence of the centers of gravity of the two components, and (c) the second moments M_2 of the two components.

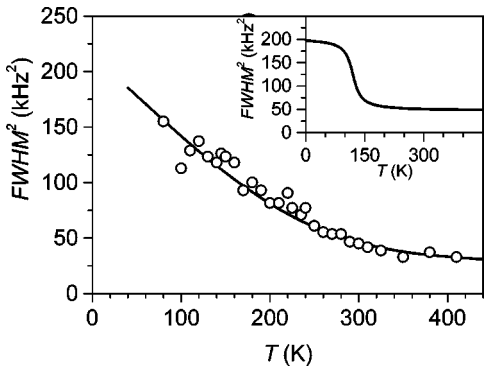

FIG. 7. The T dependence of the FWHM of the ^{207}Pb NMR line shape in PMN at orientation $[001]\|\vec{B}_0$. The inset shows the plot of the FWHM temperature dependence for the case of a simple motional transition as described by Eq. (68′) of Abragam (Ref. 17) using the value of the mean correlation time τ determined by the ^{207}Pb T_1 minimum.

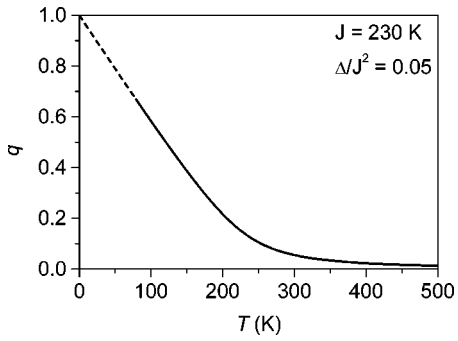

FIG. 8. Temperature dependence of the Edwards-Anderson order parameter q as determined from the ^{207}Pb NMR line shape in PMN for the orientation $[001]\|\vec{B}_0$.

ization directions—and thus directions of the largest principal axes of the anisotropic chemical shift tensors—are equally probable and the local polarization distribution function is the one predicted by the SRBRF model [expressions (5) and (6)]. This model corresponds to the spherical-shell-type distribution of the ^{207}Pb ionic shifts from their high-symmetry perovskite positions. According to the second [Fig. 1(ii)] one the shifts are discrete and allowed along the directions of the cubic axes [100], [010], and [001]. As can be seen the spherical shell SRBRF model gives a somewhat better agreement with the experiment. Here we assumed that the distribution of the isotropic part of the chemical shift tensor is of the same form as at high temperatures, i.e., a Gaussian distribution with a mean value 1000 ppm and a second moment 0.16×10^6 ppm^2. The anisotropic part of the chemical shift tensor was assumed to depend linearly on the local polarization $\sigma_a=\sigma_{a0}p$, where $\sigma_{a0}=-10^3$ ppm. Only the zeroth-order term in the expansion (19b) has been taken into account. It should be mentioned that similar calculations have been also made for the case that the ion shifts and the directions of the largest principal axes of the chemical shift tensor are pointing along the cubic body diagonals [111], $[11\bar{1}]$, $[1\bar{1}1]$, and $[\bar{1}11]$ as well as along the face diagonals [110], $[1\bar{1}0]$, [101], $[10\bar{1}]$, [011], and $[01\bar{1}]$. The agreement with experiment was here not as good as in the spherical shell ^{207}Pb displacement model.[4]

It should be mentioned that the spectral shape is definitively not powder like[15] and has no singularities as expected if we would have a completely random distribution of the orientations of the σ_a tensors of equal magnitude. This means that at any given instant of time we have a distribution of polar clusters characterized by a local polarization which varies both in orientation as well as in magnitude. This is compatible with the SRBRF model.

C. Temperature dependence of ^{207}Pb and ^{93}Nb second moments

The temperature dependence of the full width at half maximum (FWHM) of the total ^{207}Pb NMR spectrum at $[001]\|\vec{B}_0$ is shown in Fig. 7. The width varies between 30 kHz at 400 K and 150 kHz at 80 K. A comparison with the data of Laguta *et al.*[14] obtained at lower magnetic fields shows that the width of the ^{207}Pb spectrum increases with increasing magnetic field as indeed expected for the case that the width is determined by the chemical shift interactions.

As can be seen from Figs. 7 and 6(c) the width $\Delta\nu$ of the ^{207}Pb NMR spectrum—as well as the widths of the two components at those orientations where they can be resolved—start to increase sharply with decreasing temperature below 300 K, i.e., in the region of the relaxor transition. The increase in width occurs above the temperature of the ^{207}Pb T_1 minimum; i.e., it occurs in the ''fast-motion regime'' where $\omega_L\tau\ll1$ as well as $2\pi\Delta\nu\tau\ll1$. This definitely excludes the possibility that the above increase in width—and in second moment—is a motional effect. If we would deal with a motional averaging effect taking place at the transition from the fast- to the slow-motion regime, the width would be temperature independent down to 120 K where a sharp increase in the FWHM would take place. This case—which obviously does not correspond to the physical situation in PMN—is illustrated in the inset to Fig. 7 where the dotted line is calculated for the case of a motional transition according to Eq. (68′) of Abragam[17] using the mean value of the correlation time τ deduced from the ^{207}Pb T_1 minimum. The observed temperature dependence of the ^{207}Pb FWHM as well as of the corresponding second moment and its increase with decreasing temperature in the fast-motion regime is, however, typical for glassy ordering and demonstrates the presence of a kind of a glass transition in PMN. The observed Gaussian line shape of each of the two components which reflects the local polarization distribution function $W(p)$ is of the type predicted by the SRBRF model. It is drastically different from the one observed in proton or deuteron glasses, demonstrating that PMN is a ''spherical glass'' rather than an Ising-type dipolar glass. The temperature dependence of the second moment shown in Fig. 7 as well agrees with the temperature dependence of the Edwards-Anderson order parameter q predicted by the SRBRF model. One should also note that the glass transition in PMN is not sharp; i.e., we do not have $q=0$, $T>T_f$ and $q\neq0$, $T<T_f$. This is due to the presence of random fields.

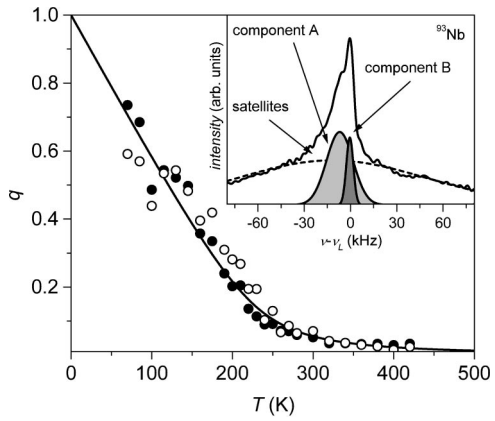

FIG. 9. Temperature dependence of q as derived from the ^{93}Nb NMR for the component A (solid circles) and component B (open circles) and fit with the SRBRF model (solid line) with parameters $J/k=230$ K and $\Delta/J^2=0.05$. The inset shows the decomposition of the ^{93}Nb line shape in two central transition components and a background due to satellite transitions.

It is important to mention that the total second moment of the ^{207}Pb frequency distribution is the sum of a temperature-independent contribution due to substitutional disorder which determines the NMR line shape at high temperatures and a temperature-dependent distribution due to polar clusters which is related to the Edwards-Anderson order parameter and which dominates the NMR line shape at lower temperatures:

$$M_2=M_2^{\text{substitutional}}+M_2^{\text{polar clusters}}. \tag{29}$$

The contribution to M_2 due to the substitutional disorder in this PMN crystal is obtained from the limiting high-temperature line shape as $M_2=90$ kHz^2.

The T dependences of the two separate Gaussian components of the ^{207}Pb NMR spectra shown in Fig. 6 can be described by the SRBRF model with $J/k=230$ K and $\Delta/J^2=0.05$. The corresponding T dependence of the Edwards-Anderson order parameter q, describing the relaxor transition in PMN, is shown in Fig. 8.

It is important to note that the fit parameters $J/k=230$ K and $\Delta/J^2=0.05$ used to describe the ^{207}Pb spectrum located at an A-type mixed perovskite site are identical to the ones obtained from the corresponding B-site $1/2\leftrightarrow -1/2$ ^{93}Nb NMR spectra (Fig. 9). Here too the central $1/2\leftrightarrow -1/2$ transition at $[001]\|\vec{B}_0$ can be decomposed into two components with an intensity ratio 4:1. The $1/2\leftrightarrow -1/2$ spectrum is here superimposed on the broad background due to $1/2\leftrightarrow 3/2,3/2\leftrightarrow 5/2,\ldots$ satellite transitions, which are absent in the Pb($I=1/2$) NMR spectrum.

Three other important facts should be stressed.

(1) No strong sharp T-independent line at the Larmor frequency corresponding to the nonpolar cubic matrix has been found in PMN either in the ^{207}Pb or the ^{93}Nb NMR spectra. This means that on the NMR time scale the system cannot be considered as consisting of static polar clusters embedded in a static nonpolar cubic matrix, but that at any given instant of time the NMR snapshot picture reveals a distribution of polar clusters with variable orientations and magnitudes of the local polarizations. The clusters are dynamic entities which exist for a certain amount of time, then disappear, and reappear in a different form. The exchange is only local so that different frequency components arise from different parts of the crystal and the total NMR spectrum is an inhomogeneous frequency distribution. On a longer time scale the effects partially average out leading to the appearance of polar clusters embedded in a nonpolar matrix.

(2) The observed orientation independence of the NMR line shape in the homogeneously disordered part of PMN both above and below the relaxor transition agrees with the SRBRF model. The angular dependence of the line arising from the presumably chemically ordered part of the crystal can be, on the other hand, understood [Fig. 1(ii)] by the fact that the longest principal axes of the chemical shift tensors here point along discrete directions.

(3) At $T=15$ K we may not anymore be in the fast-motion regime so that the nuclei do not ''see'' the time-averaged value of the local ordering field but rather its instantaneous value. The NMR spectrum $f(\nu)$, which measures the number of nuclei in a given frequency interval, here does not reflect the local polarization distribution function $W(\vec{p})$ but is rather given by

$$f(\nu)=\frac{1}{\sqrt{2\pi\alpha^2}}\exp\left[-\frac{(\nu-\nu_0)^2}{2\alpha^2}\right] \tag{30}$$

if ν is linear in $\vec{S}_i$ (see the Appendix). The fact that $f(\nu)$ is continuous and Gaussian also in the slow-motion limit and not discrete—as in the case of deuteron glasses—as well supports the basic assumption of the SRBRF model.

V. CONCLUSIONS

On the basis of the above data the following conclusions can be made.

(1) Both the A-site (^{207}Pb) and B-site (^{93}Nb) NMR spectra of a PMN single crystal are frequency distributions $f(\nu)$ which can be well described by the SRBRF model reflecting the existence of polar clusters. The local polarization distribution function in particular is Gaussian in agreement with the SRBRF model. The temperature dependence of the second moment of $f(\nu)$ and of the Edwards-Anderson order parameter q can be as well described by the SRBRF model. Thus PMN is a ''spherical glass'' rather than an Ising-type dipolar glass.

(2) The second moments M_2 of both ^{207}Pb and ^{93}Nb NMR spectra start to increase rapidly with decreasing temperature below the relaxor transition in the region of the ^{207}Pb and ^{93}Nb T_1 minima, i.e., in the fast-motion regime, where $2\pi\Delta\nu\tau\ll 1$. This shows that the increase of M_2 with decreasing T in the region of the relaxor transition in PMN is connected to a glass transition involving a change in the local polarization distribution function $W(p)$ and is not a motional transition.[15]

(3) The ^{207}Pb($I=1/2$) NMR spectra are reflecting the distribution of the anisotropic ^{207}Pb chemical shift tensors according to the spherical shell model of the ^{207}Pb ion shifts.

The ^{93}Nb($I=9/2$) NMR spectra, on the other hand, are mainly reflecting the corresponding distributions of the off-center shifts of the ^{93}Nb ions. Both ^{207}Pb and ^{93}Nb NMR spectra yield identical T dependences of q. The corresponding random bond coupling is $J=230$ K and the random field variance is $\Delta/J^2=0.05$.

(4) The fact that in PMN no separate T-independent δ-function-like central NMR line has been observed either in the ^{207}Pb or ^{93}Nb NMR spectra at the Larmor frequencies demonstrates that on the NMR time scale we cannot describe the relaxor as consisting of static polar nanoregions embedded in a nonpolar cubic matrix. At any given instant of time we have a dynamic distribution of polar clusters with variable orientation and magnitude of the local polarization, which varies in time so that the observed NMR spectrum is an average over the NMR time scale. The clusters and ionic shifts are static on the neutron scattering time scale 10^{-12} s but are dynamic entities on the NMR time scale 10^{-4}–10^{-5} s which exist for a certain amount of time, disappear, and then reappear in a different form.

APPENDIX: NMR LINE SHAPE IN THE SLOW-MOTION LIMIT AT $T\rightarrow 0$

For simplicity we consider here the uniaxial case $-\infty<S_i<\infty$, where the scalar variables S_i satisfy the spherical condition $\Sigma_{i=1}^{N}S_i^2=N$. We further assume that the NMR frequency at a given site is linearly related to the instantaneous value of the ordering field S_i:

$$\nu_i=\nu_0+\alpha S_i. \tag{A1}$$

A generalization to the vector model is easily made.

In the slow-motion limit the NMR nucleus ''sees'' the instantaneous value of the field S_i. Assuming that all values S_i have the same probability the inhomogeneous line shape is given by

$$f(\nu)=A_N\int\left(\prod_{i=1}^{N}dS_i\right)\frac{1}{N}\sum_j\delta(\nu-\alpha S_j)\delta\left(\sum_i S_i^2-N\right). \tag{A2}$$

Here we have replaced $\nu-\nu_0$ by ν and introduced a normalization constant A_N, which is determined by the relation

$$A_N^{-1}=\int\left(\prod_i dS_i\right)\delta\left(\sum_i S_i^2-N\right). \tag{A3}$$

Introducing N-dimensional spherical coordinates we have

$$A_N^{-1}=\Omega_N\int_0^\infty dS\,S^{N-1}\delta(S^2-N), \tag{A4}$$

where $\Omega_N=2\pi^{N/2}/\Gamma(N/2)$ is the N-dimensional solid angle and $\Gamma(x)$ represents the gamma function. Equation (A4) then yields

$$A_N=\frac{2}{\Omega_N N^{(n-2)/2}}. \tag{A5}$$

Returning to Eq. (A2), we note that each term in the sum over j yields the same contribution. Choosing $j=N$ we then carry out the integration over S_N and find

$$f(\nu)=\frac{A_N}{\alpha}\int\left(\prod_{i=1}^{N-1}dS_i\right)\delta\left(\sum_{i=1}^{N-1}S_i^2-N+\nu^2/\alpha^2\right). \tag{A6}$$

We now introduce $(N-1)$-dimensional spherical coordinates and rewrite Eq. (A6) as

$$f(\nu)=\frac{A_N}{\alpha}\Omega_{N-1}\int_0^\infty dS\,S^{N-2}\delta(S^2-N+\nu^2/\alpha^2). \tag{A7}$$

The integral is easily evaluated, yielding

$$f(\nu)=\frac{1}{\sqrt{\pi}\alpha}e^{-1/2}\frac{\Gamma\left(\frac{N}{2}\right)(N-\nu^2/\alpha^2)^{(N-3)/2}}{\Gamma\left(\frac{N-1}{2}\right)N^{N/2-1}}. \tag{A8}$$

Since $N\gg 1$ we can apply the Stirling formula $\Gamma(x)\approx e^{-x}x^{x-1/2}\sqrt{2\pi}$ and obtain

$$f(\nu)=\frac{1}{\sqrt{2\pi}\alpha}e^{-1/2}\frac{(N-\nu^2/\alpha^2)^{(N-3)/2}}{N^{(N-3)/2}}\left(\frac{N}{N-1}\right)^{1/2}. \tag{A9}$$

In the limit $N\rightarrow\infty$ we use the standard relation $\lim_{N\rightarrow\infty}(1-z/N)^N=\exp(-z)$, and after replacing $\nu\rightarrow\nu-\nu_0$ we arrive at the result (30). The same result is obtained if instead of a uniform distribution of S_i values one assumes a Gaussian distribution of arbitrary width.

[1] P. Boneau, P. Garnier, G. Calvarin, E. Husson, J. R. Gavarri, A. W. Hewat, and A. Morell, J. Solid State Chem. **91**, 350 (1991).

[2] E. Husson, L. Abello, and A. Morell, Mater. Res. Bull. **25**, 539 (1990).

[3] G. Burns and F. H. Dacol, Ferroelectrics **104**, 25 (1990).

[4] S. Vakhrushev, S. Zhukov, G. Fetisov, and V. Chernyshov, J. Phys.: Condens. Matter **6**, 4021 (1994).

[5] V. Westphal, W. Kleemann, and M. D. Glinchuk, Phys. Rev. Lett. **68**, 847 (1992).

[6] A. K. Tagantsev and A. E. Glazounov, J. Korean Phys. Soc. **32**, S951 (1998).

[7] D. Viehland, S. J. Jang, L. E. Cross, and M. Wuttig, J. Appl. Phys. **68**, 2916 (1990); Phys. Rev. B **46**, 8003 (1992).

[8] V. Bobnar, Z. Kutnjak, R. Pirc, R. Blinc, and A. Levstik, Phys. Rev. Lett. **25**, 5892 (2000).

[9] R. Pirc and R. Blinc, Phys. Rev. B **60**, 13 470 (1999).

[10] R. Blinc, J. Dolinšek, A. Gregorovič, B. Zalar, C. Filipič, A.

Levstik, and R. Pirc, Phys. Rev. Lett. **83**, 424 (1999).
[11] L. A. Bursil, H. Quian, J. Peng, and X. D. Fan, Physica B **216**, 1 (1995).
[12] M. A. Akbas and P. K. Davies, J. Am. Ceram. Soc. **80**, 2933 (1997).
[13] Y. Yan, S. J. Pennycook, Z. Xu, and D. Viehland, Appl. Phys. Lett. **72**, 3145 (1998).
[14] V. V. Laguta, M. D. Glinchuk, I. P. Bykov, and J. J. Van Der Klink, Ferroelectrics **156**, 273 (1994).
[15] A. Abragam, *The Principles of Nuclear Magnetism* (Oxford University Press, New York, 1960).
[16] J. Seliger, J. Magn. Reson., Ser. A. **103**, 175 (1993).
[17] A. Abragam, *The Principles of Nuclear Magnetism* (Ref. 15), p. 456.